

# Exotic Magnetic Order in the Orbital-Selective Mott Regime of Multiorbital Systems

Julián Rincón,<sup>1,2</sup> Adriana Moreo,<sup>2,3</sup> Gonzalo Alvarez,<sup>1,4</sup> and Elbio Dagotto<sup>2,3</sup>

<sup>1</sup>Center for Nanophase Materials Sciences, Oak Ridge National Laboratory, Oak Ridge, Tennessee 37831, USA

<sup>2</sup>Materials Science and Technology Division, Oak Ridge National Laboratory, Oak Ridge, Tennessee 37831, USA

<sup>3</sup>Department of Physics and Astronomy, The University of Tennessee, Knoxville, Tennessee 37996, USA

<sup>4</sup>Computer Science & Mathematics Division, Oak Ridge National Laboratory, Oak Ridge, Tennessee 37831, USA

(Dated: November 12, 2018)

The orbital-selective Mott phase (OSMP) of multiorbital Hubbard models has been extensively analyzed before using static and dynamical mean-field approximations. In parallel, the properties of Block states (antiferromagnetically coupled ferromagnetic spin clusters) in Fe-based superconductors have also been much discussed. The present effort uses numerically exact techniques in one-dimensional systems to report the observation of Block states within the OSMP regime, connecting two seemingly independent areas of research, and providing analogies with the physics of Double-Exchange models.

PACS numbers: 71.30.+h, 71.27.+a, 71.10.Fd, 71.10.Fd

**Introduction.** The combined interplay of charge, spin, lattice, and orbital degrees of freedom have led to an enormous variety of emergent phenomena in strongly correlated systems. A prototypical example is the half-filled single-orbital metal-insulator transition, that is realized in materials such as  $\text{La}_2\text{CuO}_4$ , a parent compound of the Cu-based high temperature superconductors. If several active orbitals are also considered in the study of this transition, an even richer phase diagram is anticipated, where states such as band insulators, correlated metals, and orbital-selective Mott phases (OSMP) can be stabilized. In particular, the study of the OSMP and its associated orbital-selective Mott transition has attracted considerable attention in recent years [1–3].

The OSMP is a state where even though Mott insulator (MI) physics occurs, it is restricted to a subset of all the active orbitals present in the problem. This state has narrow-band localized electrons related to the MI orbitals, coexisting with wide-band itinerant electrons at the other orbitals [4–6]. To stabilize the OSMP, a robust Hund interaction  $J$  is needed. In general, the hybridization within orbitals  $\gamma$ ,  $V_{\gamma,\gamma'}$ , and crystal fields,  $\Delta_\gamma$ , work against  $J$  since they favor low-spin ground states. Therefore, if  $J \gg \Delta_\gamma$ ,  $V_{\gamma,\gamma'}$ , the OSMP is expected to be stable and display robust local moments [6].

Several studies focused on the effects of interactions, filling fractions, etc., on the stability of orbital-selective phases [3]. This previous theoretical work was performed within mean-field approximations (such as Dynamical Mean Field Theory [4–8], slave-spins [6, 8–11], or Hartree-Fock [12, 13]). Using these methods the OSMP stability conditions have been established. However, to our knowledge, there have been no detailed studies of the influence of full quantum fluctuations on this phase and therefore, and more importantly for our purposes, of their low-temperature electronic and magnetic properties.

Recently, these issues received considerable attention in the Fe-based superconductors community. In this context, multiorbital models containing Hubbard  $U$  and  $J$  interactions, as well as crystal-field splittings, are widely employed, and the existence of OSMP regimes has been extensively investi-

gated [6, 7, 9, 10, 12–17]. For these reasons, our models are chosen to resemble qualitatively models for pnictides and selenides, so that our conclusions could be of potential relevance in that context.

Our aim is two-fold: (i) By employing techniques beyond mean-field to study the phase diagrams of three-orbital Hubbard models, the robustness of the OSMP to full quantum fluctuations can be confirmed via numerical simulations. (ii) More importantly, once the stability of this state has been established, its charge and magnetic orders can be explored. Our main result is that full ferromagnetic (FM) and exotic “Block” states have been found to be stable within the OSMP regime. Block phases, such as the antiferromagnetic (AFM) state made of  $2 \times 2$  FM-clusters, were discussed extensively in the selenides literature mainly in the presence of iron vacancies [18–26] or in special geometries such as two-leg ladders [27–29], but not in the OSMP framework. Our new results suggest that the concepts of OSMP and Block phases, until now separately considered, are actually related after showing that Block states are stabilized *within* the OSMP regime.

Our study is performed in a one-dimensional geometry. This restriction arises from the need to employ accurate techniques such as the Density Matrix Renormalization Group (DMRG) [30–32]. Thus, our conclusions are only *suggestive* of similar physics in the layered Fe-based superconductors, and only further work can confirm this assumption. However, there are real quasi one-dimensional materials, such as the previously mentioned ladders [27–29], that may provide a direct physical realization of our results.

**Model.** The Hamiltonians used are multiorbital Hubbard models composed of kinetic energy and interacting terms:  $H = H_K + H_{\text{int}}$ . The kinetic contribution is written as

$$H_K = - \sum_{i\sigma\gamma\gamma'} t_{\gamma\gamma'} (c_{i\sigma\gamma}^\dagger c_{i+1\sigma\gamma'} + \text{H.c.}) + \sum_{i\sigma\gamma} \Delta_\gamma n_{i\sigma\gamma}, \quad (1)$$

where  $t_{\gamma\gamma'}$  denotes a (symmetric) hopping amplitude defined in orbital space  $\{\gamma\}$  connecting the lattice sites  $i$  and  $i + 1$  ( $\gamma = 0, 1, 2$ ) of a one dimensional lattice of length  $L$ . The

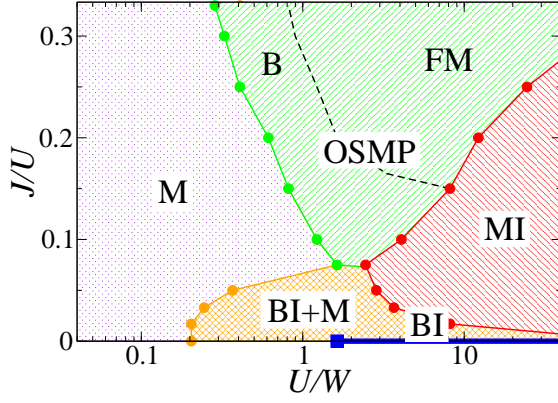


FIG. 1. Phase diagram of the three-orbital Model 1 for  $n = 4/3$ . The different phases are labeled as: metal (M), band insulator (BI), a metallic state resembling the BI state (BI+M), Mott insulator (MI), and orbital-selective Mott phase (OSMP). Within the OSMP regime, it is possible to distinguish between Block (B) and FM states.

hopping amplitudes used here are (eV units):  $t_{00} = t_{11} = -0.5$ ,  $t_{22} = -0.15$ ,  $t_{02} = t_{12} = 0.1$ , and  $t_{01} = 0$ , with an associated total bandwidth  $W = 4.9|t_{00}|$  (the individual orbital bandwidths  $W_\gamma/|t_{00}|$  are 3.69, 3.96, and 1.54, for  $\gamma = 0, 1$ , and 2, respectively). Both hoppings and  $W$  are comparable in magnitude to those used in more realistic pnictides models [33]. Only hybridizations between orbitals 0 and 2, and 1 and 2, are considered.  $\Delta_\gamma$  defines a crystal-field splitting which is orbital-dependent with values  $\Delta_0 = -0.1$ ,  $\Delta_1 = 0$ , and  $\Delta_2 = 0.8$ . All these parameters are *phenomenological*, i.e. not derived from *ab-initio* calculations. Their values were chosen so that the band structure [shown in the inset of Fig. 2(a)] qualitatively resembles that of higher dimensional pnictides, with a hole pocket at  $k = 0$  and electron pockets at  $k = \pm\pi$ . This model will be referred to as “Model 1” while a “Model 2” with slightly different parameters will be discussed in the Suppl. Material (SM) [34]. The Coulombic repulsion interacting portion of the Hamiltonian is

$$H_{\text{int}} = U \sum_{i\gamma} n_{i\uparrow\gamma} n_{i\downarrow\gamma} + (U' - J/2) \sum_{i\gamma < \gamma'} n_{i\gamma} n_{i\gamma'} - 2J \sum_{i\gamma < \gamma'} \mathbf{S}_{i\gamma} \cdot \mathbf{S}_{i\gamma'} + J \sum_{i\gamma < \gamma'} (P_{i\gamma}^+ P_{i\gamma'} + \text{H.c.}), \quad (2)$$

containing the standard intra-orbital Hubbard repulsion,  $U$ , and Hund’s rule coupling,  $J$ . For  $SU(2)$  symmetric systems, the relation  $U' = U - 2J$  holds.  $c_{i\sigma\gamma}$  annihilates an electron with spin  $\sigma$  at orbital  $\gamma$  and site  $i$ , and  $n_{i\sigma\gamma}$  counts electrons at  $i$  with quantum numbers  $(\sigma, \gamma)$ . The operator  $\mathbf{S}_{i\gamma}$  ( $n_{i\gamma}$ ) is the spin (total electronic density) at orbital  $\gamma$  and site  $i$ ; and the definition  $P_{i\gamma} = c_{i\downarrow\gamma} c_{i\uparrow\gamma}$  was introduced. The electronic density per orbital is fixed to  $n = 4/3$ , i.e., four electrons every three orbitals, in analogy with the filling used in the modeling of iron superconductors with three orbitals [33]. As many-body technique, the DMRG method [30–32] was used, with technical details provided in the SM [34].

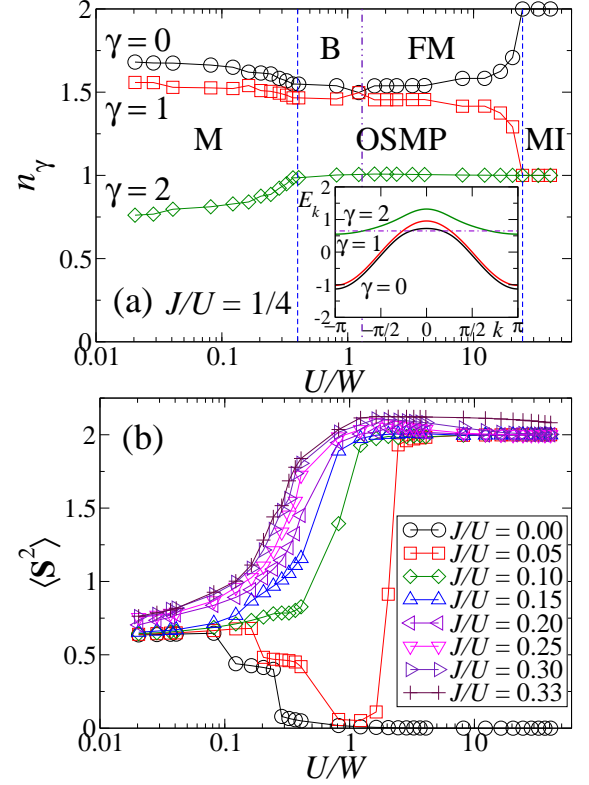


FIG. 2. Results for Model 1: (a) Electronic occupancy,  $n_\gamma$ , corresponding to orbital  $\gamma$  vs.  $U$  in bandwidth  $W$  units, at  $J/U = 1/4$ , and for  $L = 24$ . Inset: Band structure of Model 1 (eV units). Violet (dash dotted) line is the  $n = 4/3$  Fermi level. (b) Mean value of the square of the total spin at each site, at several values of  $J/U$ . Within the OSMP, a robust magnetic moment is observed.

**Results.** In Fig. 1, the phase diagram of Model 1 is shown, based on the DMRG measurements of the orbital occupancies  $n_\gamma$  and the square of the spin operator at every site (see Fig. 2). Two phases are obvious: a metallic weakly interacting state M at small  $U$  and a MI regime at large  $U$ , where  $n_0 = 2$ ,  $n_1 = n_2 = 1$  minimize the double-occupancy energy penalization and  $J$  induces a spin 1 state at each site (orbital 0 is doubly occupied because of the small but nonzero split between orbitals 1 and 0). Naturally, the spin order is staggered in the MI phase. Less obvious are the other two phases in Fig. 1. For example, a correlated “band insulator” (BI) with  $n_0 = n_1 = 2$  and  $n_2 = 0$  is found in a region bounded by  $J$  less than the crystal-field splittings  $\Delta_\gamma$ , so that the low-spin state is favored, and  $U/W$  not too large, so that double occupancy is not heavily suppressed by  $U$ . At  $J$  exactly 0.0, the BI state survives for any value of  $U/W$  because in this line  $U = U'$ . But at large  $U/W$ , a tiny  $J$  is sufficient to destabilize the BI state into the MI state. The related BI+M state has  $n_0 \sim n_1 \sim 2$  and  $n_2 \sim 0$ : a metallic state with characteristics close to the BI [35]. Clearly, increasing  $J/U$  the BI/BI+M phases are suppressed. In fact, with increasing  $U/W$  the M state is the most stable at  $J/U \sim 0.075$  because of the competition  $J$  vs.  $\Delta_\gamma$ . Since the BI/BI+M states are not our main

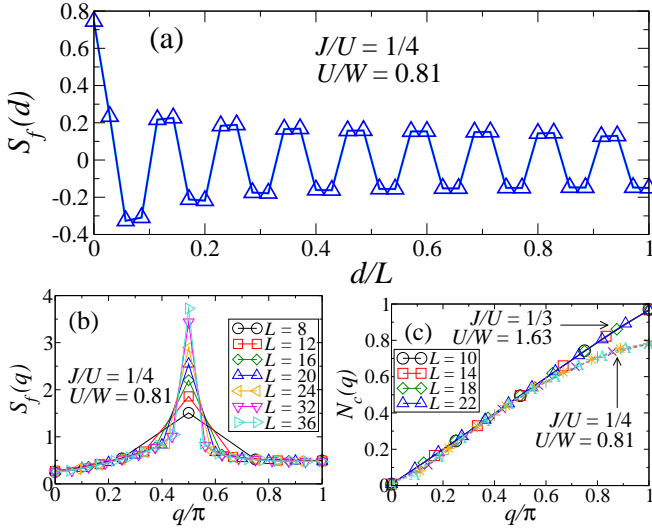


FIG. 3. (a) Spin correlations in the localized (insulating) band vs. the normalized distance, at  $J/U = 1/4$ ,  $U/W = 0.81$ , and  $L = 36$ . The formation of ferromagnetic clusters interacting antiferromagnetically is clearly shown. (b) Spin structure factor for panel (a) at several  $L$ 's (symbols). A clear peak at  $q/\pi = 1/2$  is shown. (c) Charge structure factor of the itinerant bands for the  $J/U$  and  $U/W$  indicated, and varying  $L$  (symbols).

focus, additional properties are in the SM [34].

Our most important result in Fig. 1 is the presence of a prominent OSMF regime, stabilized after  $J$  becomes larger than a threshold that depends on  $\Delta_\gamma$ . The OSMF contains the region  $J/U \sim 1/4$  at intermediate  $U/W$  believed to be realistic [36–39]. For the prototypical value  $J/U = 1/4$ , in the small- $U$  metallic regime the  $n_\gamma$  values evolve smoothly from the non-interacting limit. However, at a critical  $U/W$ , the  $\gamma = 2$  orbital population reaches 1 and stays there in a wide window of couplings, while the other two densities develop a value  $\sim 1.5$  [Fig. 2(a)]. These results are robust against changes in  $L$  and they are compatible with the presence of an OSMF, that eventually ends at a second critical  $U/W$  when the transition to the MI regime occurs. In the SM [34], results similar to Fig. 2 (a) but adding two holes are shown: while  $n_2$  remains at 1 in the OSMF regime, now  $n_0 \sim n_1 \sim 1.37$ , showing that  $n_0$  and  $n_1$  evolve with doping while  $n_2$  is locked as expected in the OSMF [40]. The formation of a robust local moment in the OSMF is shown in Fig. 2(b). These DMRG results confirm the presence of the OSMF even with full quantum fluctuations incorporated. The OSMF regime is eventually suppressed by decreasing  $J/U$ : at weak  $U/W$  coupling because of the competition with  $\Delta_\gamma$  that favors the M and BI+M states, and at strong  $U/W$  coupling because of the competition with the MI state.

While previous mean-field studies of the OSMF arrive to conclusions qualitatively similar to those of Fig. 2, the DMRG method can reveal the fine details of the OSMF spin and charge arrangements. For example, Fig. 3(a) contains representative OSMF spin-spin correlation functions [34]. Surpris-

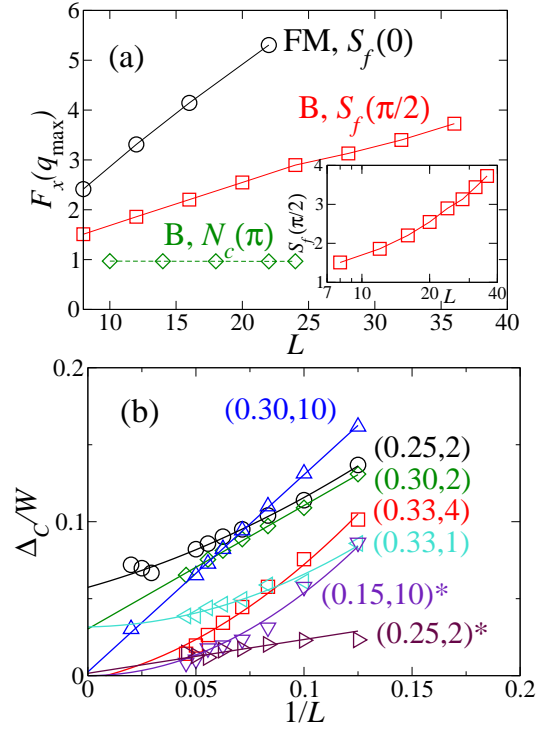


FIG. 4. (a) Size dependence of the peaks of the charge (dashed line) and spin (solid line) structure factors for the FM and B phases with couplings  $J/U = 1/4$ ,  $U/W = 0.81$  and  $J/U = 1/3$ ,  $U/W = 1.63$ , respectively. Inset: Semi-logarithmic plot of  $S_f(\pi/2)$ . (b) Charge gap vs.  $1/L$  for the values of the pair  $(J/U, U)$  shown. Results with the “\*” symbol stand for the 2-hole doped case.

ingly, an unexpected pattern of spins  $\uparrow\uparrow\downarrow\downarrow$  is clearly observed. The spin structure factor in Fig. 3(b) displays a sharp peak at  $q = \pi/2$ , that increases with  $L$  (the peak is also robust away from  $n = 4/3$ ). Then, at intermediate couplings, our DMRG results indicate that exotic Block spin states can be stabilized within the OSMF (region “B” in Fig. 1). These Block spin states are qualitatively similar to those reported for pnictides and selenides [18–29].

In addition, a surprising FM OSMF region with a maximal value of the spin has been found (see SM [34]). Its charge structure factor,  $N_c(q)$ , is shown in Fig. 3(c) at several  $L$ 's. Although there are no signs of charge order, there is a clear evidence of spinless fermions behavior with momentum  $q = \pi$ . The effective filling of the emergent spinless fermions can be understood by considering that there are three electrons per site in the itinerant bands (and one in the localized band). This is equivalent to one hole per site per two orbitals or, equivalently,  $1/2$  hole per site on an effective chain of length  $2L$ . This is a “half-filled” spinless fermion system, inducing the momentum of  $\pi$  in  $N_c(q)$ . For the B phase,  $N_c(q)$  shows a qualitatively similar behavior, no charge order, and a spectrum broadening as shown in Fig. 3 (c) [34].

Figure 4(a) shows the finite-size dependence of the peak of the charge and spin structure factors, generically referred to as  $F_x(q_{\max})$ , for the B and FM regions.  $F_x$  becomes  $S_f$  and

$N_c$  for spin and charge, respectively, at the maximal momentum  $q_{\max}$ . The FM state displays a quasi-linear increase of the structure factor peak vs.  $L$  signaling a quasi-long range order in the spin correlations. The B phase presents a logarithmic increase with  $L$  indicating, again, (quasi-long-ranged) power-law behavior of the spin correlations with non-trivial exponents [see inset Fig. 4(a)]. On the other hand, the charge peak shows no order tendencies in any of the phases evidencing only short-ranged correlations; however, the charge correlations show a non-trivial trend associated with spinless behavior, as discussed in Fig. 3(c).

The metallic vs. insulating nature of the OSMP is difficult to address, but guidance can be obtained by studying the charge gap  $\Delta_C$  [34] [see Fig. 4(b)]. While the extrapolation to the bulk is difficult, “by eye” it is clear that the extrapolations appear to converge to small gaps in the  $0.05 \times W$  to  $0.00$  range. Moreover, upon light 2-hole doping the gap vanishes. Thus, a likely scenario is that the Block states at exactly  $n = 4/3$  have a small gap, that rapidly closes with doping. Since in the realistic five-orbital Hubbard model for pnictides the combined population of the  $xz$ ,  $yz$ , and  $xy$  orbitals is not exactly 4, the relevant OSMP regime would be metallic.

*Relation to Kondo lattice models.* The results reported here unveil interesting analogies with previous studies of the Double Exchange (DE) models for Mn-oxides [41]. This is natural, since DE physics relies on the interplay of localized and itinerant degrees of freedom, as it occurs in the OSMP regime. This DE-OSMP relation is rigorous: for the case of a two-band model, it has been shown that the low-energy effective theory of the OSMP is related to a FM Kondo lattice model (FMKLM) with Hubbard repulsion in the conduction band [5]. For a generic multiorbital case, one can show that the effective model turns into a “correlated” FMKLM. If the system has  $n_{\text{orb}}$  orbitals, this model describes the FM exchange between the localized band with magnetic moments and a many-body bath of itinerant electrons. The bath is built out of the remaining  $n_{\text{orb}} - 1$  orbitals and the only interaction between localized and itinerant bands is the FM exchange.

This DE-OSMP relation provides further support to the main conclusions of our effort. In fact, previous DMRG and Monte Carlo investigations of the DE model already unveiled a variety of so-called “island phases” containing small clusters of various shapes made of ferromagnetically aligned spins and with AFM couplings among them, both in one and two dimensions [42–45]. These phases are qualitatively the analog of the Block phases, although for quite different couplings, electronic densities, and band structures. The previous DE results [42–45] reinforces our conjecture that the Block states observed here via the detailed analysis of examples are likely stable for a wider variety of models, both in one and two dimensions. Since in manganites it was shown that exotic non-FM phases need the crucial addition of a superexchange coupling  $J_{\text{AFM}}$  between the localized spins [41, 46, 47], it is natural to conjecture that a similar coupling must be incorporated into the effective model in the OSMP regime of iron superconductors and related compounds.

*Conclusions.* In this publication, multiorbital Hubbard models have been investigated using DMRG techniques in one dimension, and the phase diagrams have been constructed. Our main result is that the OSMP regime contains unexpected internal structure. In particular, phases with the characteristics of Block states (FM clusters, AFM coupled) have been identified. Full FM has also been found within the OSMP. The Block states likely arise from the frustration generated by competing ferromagnetic/antiferromagnetic tendencies in the model, as it happens with the island phases in manganites. Block phases were discussed before in models of Fe-based superconductors, but were not associated with the OSMP regime. Moreover, since a formal mapping between the Hubbard and Kondo lattice models exists in the OSMP regime, our results establish an unexpected analogy between Double-Exchange physics, where similar Block phases were reported before, and that of multiorbital models for iron superconductors. Our conclusions are of direct relevance to real quasi one-dimensional materials but they may apply to two-dimensional systems as well, considering that “island phases” in the two dimensional Kondo models have been reported before [45].

Support by the Early Career Research Program, Scientific User Facilities Division, Basic Energy Sciences, US Department of Energy, under contract with UT-Battelle (J.R. and G.A.) and by the U.S. Department of Energy, Office of Basic Energy Sciences, Materials Sciences and Engineering Division (J.R.) is acknowledged. For this project A.M. and E.D. were supported by the National Science Foundation under Grant No. DMR-1104386.

- 
- [1] V. Anisimov, I. Nekrasov, D. Kondakov, T. M. Rice, and M. Sigrist, *Eur. Phys. J. B* **25**, 191 (2002).
  - [2] M. Vojta, *J. Low. Temp. Phys.* **161**, 203 (2010).
  - [3] A. Georges, L. de’ Medici, and J. Mravlje, *Annu. Rev. Cond. Mat. Phys.* **4**, 137 (2013).
  - [4] A. Liebsch, *Phys. Rev. B* **70**, 165103 (2004).
  - [5] S. Biermann, L. de’ Medici, and A. Georges, *Phys. Rev. Lett.* **95**, 206401 (2005).
  - [6] L. de’ Medici, S. R. Hassan, M. Capone, and X. Dai, *Phys. Rev. Lett.* **102**, 126401 (2009).
  - [7] H. Ishida and A. Liebsch, *Phys. Rev. B* **81**, 054513 (2010).
  - [8] L. de’ Medici, *Phys. Rev. B* **83**, 205112 (2011).
  - [9] R. Yu and Q. Si, *Phys. Rev. B* **86**, 085104 (2012).
  - [10] R. Yu and Q. Si, *Phys. Rev. Lett.* **110**, 146402 (2013).
  - [11] L. de’ Medici, G. Giovannetti, and M. Capone, *arXiv:1212.3966*.
  - [12] E. Bascones, B. Valenzuela, and M. J. Calderón, *Phys. Rev. B* **86**, 174508 (2012).
  - [13] B. Valenzuela, M. J. Calderón, G. León, E. Bascones, *Phys. Rev. B* **87**, 075136 (2013).
  - [14] A. Liebsch, *Phys. Rev. B* **84**, 180505(R) (2011).
  - [15] M. Yi, D. Lu, R. Yu, S. Riggs, J.-H. Chu, B. Lv, Z. Liu, M. Lu, Y. Cui, M. Hashimoto, S.-K. Mo, Z. Hussain, C.-W. Chu, I. Fisher, Q. Si, and Z.-X. Shen, *Phys. Rev. Lett.* **110**, 067003 (2013).
  - [16] N. Lanatá, H. U. R. Strand, G. Giovannetti, B. Hellsing, L. de’



- Medici, and M. Capone, Phys. Rev. B **87**, 045122 (2013).
- [17] M. Greger, M. Kollar, and D. Vollhardt, Phys. Rev. Lett. **110**, 046403 (2013).
- [18] W. Bao, Q. Huang, G. F. Chen, M. A. Green, D. M. Wang, J. B. He, X. Q. Wang, and Y. Qiu, Chin. Phys. Lett. **28**, 086104 (2011).
- [19] C. Cao, and J. Dai, Phys. Rev. Lett. **107**, 056401 (2011).
- [20] Q. Luo, A. Nicholson, J. Riera, D.-X. Yao, A. Moreo, and E. Dagotto, Phys. Rev. B **84**, 140506(R) (2011).
- [21] R. Yu, J.-X. Zhu, and Q. Si, Phys. Rev. Lett. **106**, 186401 (2011).
- [22] S.-M., Huang and C.-Yu Mou, Phys. Rev. B **84**, 184521 (2011).
- [23] W. Li, S. Dong, C. Fang, and J.-P. Hu, Phys. Rev. B **85**, 100407(R) (2012).
- [24] W.-G. Yin, C.-C. Lee, and W. Ku, Phys. Rev. Lett. **105**, 107004 (2010).
- [25] E. Dagotto, Rev. Mod. Phys. **85** 849 (2013), and references therein.
- [26] P. Dai, J.P. Hu, and E. Dagotto, Nat. Physics **8**, 709 (2012).
- [27] J. M. Caron, J. R. Neilson, D. C. Miller, A. Llobet, and T. M. McQueen, Phys. Rev. B **84**, 180409(R) (2011).
- [28] J. M. Caron, J. R. Neilson, D. C. Miller, K. Arpino, A. Llobet, and T. M. McQueen, Phys. Rev. B **85**, 180405(R) (2012).
- [29] Q. L. Luo, A. Nicholson, J. Rincón, S. Liang, J. Riera, G. Alvarez, L. Wang, W. Ku, G. Samolyuk, A. Moreo, and E. Dagotto, Phys. Rev. B **87**, 024404 (2013).
- [30] S. R. White, Phys. Rev. Lett. **69**, 2863 (1992); *ibid.* **48**, 10345 (1993).
- [31] U. Schollwöck, Rev. Mod. Phys. **77**, 259 (2005).
- [32] K. Hallberg, Adv. Phys. **55**, 477 (2006).
- [33] M. Daghofer, A. Nicholson, A. Moreo, and E. Dagotto, Phys. Rev. B **81**, 014511 (2010).
- [34] The supplementary material at [URL will be inserted by publisher] contains details of the definition of physical quantities, and additional numerical results.
- [35] This BI+M phase (not to be confused with a phase separated state involving the BI and M states) has characteristics similar to those reported at small  $J$  in R. Yu and Q. Si, Phys. Rev. B **84**, 235115 (2011). Further studies beyond the scope of the present publication can clarify its properties, as well as the true existence of a sharp transition between the M and BI+M states.
- [36] K. Haule and G. Kotliar, New J. of Phys. **11**, 025021 (2009).
- [37] Q. Luo, G. Martins, D.-X. Yao, M. Daghofer, R. Yu, A. Moreo, and E. Dagotto, Phys. Rev. B **82**, 104508 (2010).
- [38] Z. P. Yin, K. Haule, and G. Kotliar, Nat. Mater. **10**, 932 (2011).
- [39] J. Ferber, K. Foyevtsova, R. Valentí, and H.O. Jeschke, Phys. Rev. B **85**, 094505 (2012). See also Y.-Z. Zhang, Hunpyo Lee, H.-Q. Lin, C.-Q. Wu, H. O. Jeschke, and R. Valentí, Phys. Rev. B **85**, 035123 (2012), and references therein.
- [40] The inset of Fig. S6 in the SM shows that  $n_0$  and  $n_1$  are very close in the OSMP regime, but not identical. The same occurs in Fig. 2 (a). The reason is that the initial small energy splitting between levels 0 and 1 is washed out in the OSMP where  $U/W$  is of order 1 or larger.
- [41] E. Dagotto, T. Hotta, and A. Moreo, Physics Reports **344**, 1 (2001).
- [42] D. J. García, K. Hallberg, C. D. Batista, M. Avignon, and B. Alascio, Phys. Rev. Lett. **85**, 3720 (2000).
- [43] D. J. Garcia, K. Hallberg, C. D. Batista, S. Capponi, D. Poilblanc, M. Avignon, and B. Alascio, Phys. Rev. B **65**, 134444 (2002).
- [44] D. J. Garcia, K. Hallberg, B. Alascio, and M. Avignon, Phys. Rev. Lett. **93**, 177204 (2004).
- [45] H. Aliaga, B. Normand, K. Hallberg, M. Avignon, and B. Alascio, Phys. Rev. B **64**, 024422 (2001).
- [46] S. Yunoki and A. Moreo, Phys. Rev. B **58**, 6403 (1998).
- [47] A. Moreo, M. Mayr, A. Feiguin, S. Yunoki, and E. Dagotto, Phys. Rev. Lett. **84**, 5568 (2000).

# Supplementary Material for Exotic Magnetic Order in the Orbital-Selective Mott Regime of Multiorbital Systems

Julián Rincón,<sup>1,2</sup> Adriana Moreo,<sup>2,3</sup> Gonzalo Alvarez,<sup>1,4</sup> and Elbio Dagotto<sup>2,3</sup>

<sup>1</sup>Center for Nanophase Materials Sciences, Oak Ridge National Laboratory, Oak Ridge, Tennessee 37831, USA

<sup>2</sup>Materials Science and Technology Division, Oak Ridge National Laboratory, Oak Ridge, Tennessee 37831, USA

<sup>3</sup>Department of Physics and Astronomy, The University of Tennessee, Knoxville, Tennessee 37996, USA

<sup>4</sup>Computer Science & Mathematics Division, Oak Ridge National Laboratory, Oak Ridge, Tennessee 37831, USA

(Dated: November 12, 2018)

In this section, technical details concerning the numerical calculation and lattice models are provided. Also supplementary results regarding other states in the phase diagrams of the two Hamiltonians analyzed here are presented.

## S1. IMPLEMENTATION OF THE DMRG TECHNIQUE

The Density Matrix Renormalization Group (DMRG) technique [1–3] was used in this publication, with  $L$  up to 50 sites. The number of states per block kept during the DMRG iterations were 900 and up to 19 sweeps were performed during the finite-size algorithm evolution, giving rise to a discarded weight of the order  $10^{-6} - 10^{-4}$ . For small system sizes,  $L = 4$  and 6, DMRG results were confirmed by contrast against an exact diagonalization. Finite-size effects are surprisingly small in the phase diagrams reported here [4]. The full open source code, sample input decks, and corresponding computational details have been made available at <https://web.ornl.gov/~gz1/papers/49/>.

To address the accuracy of the DMRG calculations performed in this work, Fig. S1 displays the ground state energies and the height of the peaks of the spin structure factor in the Block phase as a function of the number of states kept,  $m$ , for  $L = 12$  (symbols: circles and squares) and 24 (symbols: diamonds and triangles). Mean values such as the ground state energy show a smooth, almost flat, dependence with  $m$ , as expected [2, 3]. This quantity has clearly reached convergence for the number of states used for both lengths,  $L$ , considered. However, correlation functions typically have a more complex evolution with the number of states kept. By performing quadratic fits to the data, it was observed that the error in the heights of the peaks for 12 and 24 sites correspond to 4% and 15%, respectively. This level of error is acceptable given the computational complexity of the three-orbital model worked out here. It should be remarked that within DMRG the study of a three-orbital Hubbard model on a chain of length, say,  $L = 36$  and with  $m = 800$  states is approximately equivalent to the study of a one-orbital Hubbard model using  $L = 108$  and  $m = 12800$ . This illustrates that the numerical effort presented here is substantial.

## S2. DEFINITION OF MODEL 2 AND RESULTS

To help determine how general the conclusions reported in the main text are, in the present effort two model Hamiltoni-

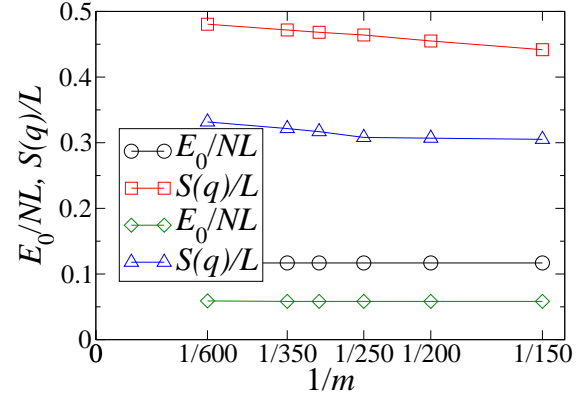


FIG. S1. Dependence of some observables with the number of states kept in the DMRG calculations,  $m$ . Shown are the ground state energy (per site and per number of electrons) and the peak height (per site) of the spin structure factor in the Block phase (evaluated at  $q = \pi/2$ ). Circles and squares are results for  $L = 12$ , while diamonds and triangles are for  $L = 24$ . All these results are for  $U/W = 0.81$ ,  $J/U = 0.25$ , and  $n = 4/3$ .

ans, that slightly differ in their band structures as shown in Fig. S2 and in the hoppings of Table S1, have been studied. These models were named Model 1 and Model 2. Although both of these models still contain a combination of hole and electron pockets, their main differences are in the size of the hole pockets. In both cases, the filling factor will be fixed to  $n = 4/3$  (i.e., four particles every three orbitals), in analogy with the  $n$  used for three-orbital models for iron superconductors, as discussed in the main text. Results for Model 1 were presented in the main text, while results for Model 2 are presented here.

Figure S3 contains the DMRG results for Model 2. Panel (a) has the phase diagram while Panel (b) displays the orbital occupations, to illustrate how the phase diagram was constructed. There are clear similarities with the results for Model 1, since the M, MI, and OSMP regimes are present.

TABLE S1. Set of parameters that define the models studied in this work. Hoppings and  $\Delta_\gamma$  were defined in the main text.

	$t_{00} = t_{11}$	$t_{02}$	$t_{12}$	$\Delta_0$	$\Delta_1$	$\Delta_2$
Model 1	-0.5	-0.15	0.1	-0.1	0.0	0.8
Model 2	-0.5	-0.25	0.1	-0.5	0.0	0.5

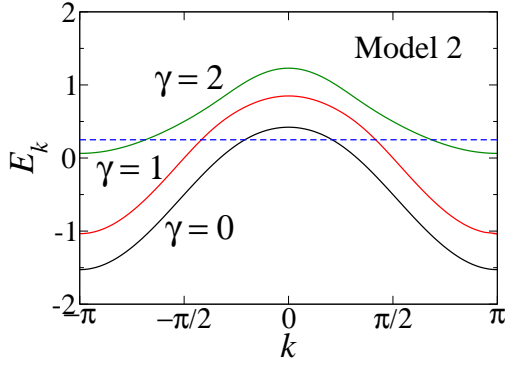


FIG. S2. The band structure of Model 2. The blue (dashed) line is the Fermi energy at  $n = 4/3$ . The bandwidth is  $W = 5.5|t_{00}|$ . The difference with Model 1 is mainly in the size of the hole pockets.

Within OSMF, there is a Block (B) region as well, although in this case the spin pattern [that can be deduced from Panel (c)] is  $\uparrow\uparrow\downarrow\downarrow$ . The Fermi surface differences presumably lead to the B-region different spin patterns between Models 1 and 2. The FM regime within the OSMF is also present in Model 2, as it is in Model 1. However, the BI+M regime is absent, and in the OSMF there is a new regime with weak magnetization in Model 2. In spite of these small differences, the general issue addressed in this publication, namely the existence of the OSMF and the presence of Block phases inside, is common to both Models 1 and 2, suggesting that these results could be generic beyond the models used here [5].

### S3. DEFINITION OF OBSERVABLES

The several phases appearing in our models have been identified by calculating expectation values and two-point correlation functions. For instance, the occupation number of each orbital, defined as

$$n_\gamma = \frac{1}{L} \sum_{i,\sigma} \langle n_{i\sigma\gamma} \rangle, \quad (\text{S1})$$

has been calculated, as well as their respective magnetizations,

$$S_\gamma^z = \frac{1}{2L} \sum_i \langle n_{i\uparrow\gamma} - n_{i\downarrow\gamma} \rangle. \quad (\text{S2})$$

With regards to correlation functions, the focus has been on the full spin and charge correlations defined as follows:

$$n_{i,j} = \langle n_i n_j \rangle, \quad (\text{S3})$$

and

$$S_{i,j} = \langle \mathbf{S}_i \cdot \mathbf{S}_j \rangle, \quad (\text{S4})$$

where  $n_i = \sum_\gamma n_{i\gamma}$  and  $\mathbf{S}_i = \sum_\gamma \mathbf{S}_{i\gamma}$ . Since there is a close relationship between the OSMF state and the ground state of a Kondo lattice model [6], as discussed in the main text, the

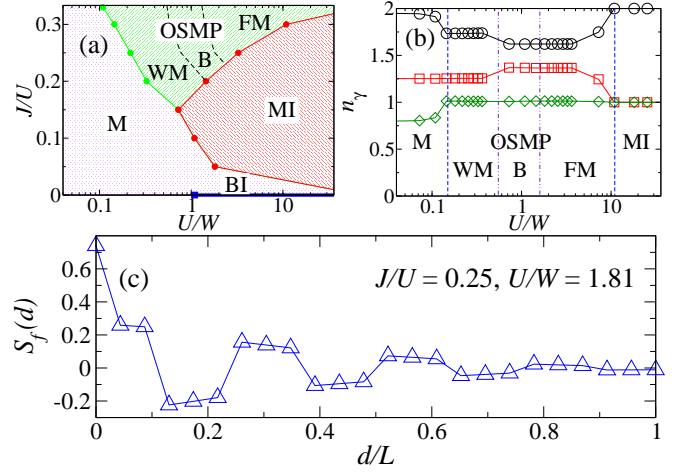


FIG. S3. Results for Model 2: (a) Phase diagram at  $n = 4/3$ . Within the OSMF there is an additional phase characterized by the presence of weak magnetism (WM). Other labels are as already defined in the main text for Model 1. (b) Orbital occupancy,  $n_\gamma$ , vs.  $U/W$ , for  $J/U = 0.30$ . The OSMF is found within the range  $0.15 < U/W < 10$ . (c) Spin correlations in the localized (insulating) band vs. distance for  $J/U = 0.25$ ,  $U/W = 1.81$ , and  $L = 24$  sites, illustrating the formation of the Block state  $\uparrow\uparrow\downarrow\downarrow$ .

charge correlations of the itinerant bands have also been evaluated,

$$N_{i,j}^c = \langle n_i^c n_j^c \rangle, \quad (\text{S5})$$

as well as the spin correlations of the Mott-insulating orbital,

$$S_{i,j}^f = \langle \mathbf{S}_i^f \cdot \mathbf{S}_j^f \rangle. \quad (\text{S6})$$

The “itinerant” charge was defined as

$$n_i^c = \sum_{\gamma=0,1} n_{i\gamma}, \quad (\text{S7})$$

and the “localized” spin as

$$\mathbf{S}_i^f = \sum_{\alpha,\beta} c_{i\beta 2}^\dagger \boldsymbol{\tau}_{\alpha\beta} c_{i\beta 2}, \quad (\text{S8})$$

with  $\boldsymbol{\tau}$  being the Pauli matrices. These quantities are defined *in the spirit* of a Kondo lattice model calculation [6].

With  $n$  being the mean value of a generic charge operator  $\mathcal{N}_j$ , the corresponding structure factors for charge and spin are defined as

$$\mathfrak{N}(q) = \frac{1}{L} \sum_{k,j} e^{-iq(j-k)} \langle (\mathcal{N}_k - n)(\mathcal{N}_j - n) \rangle, \quad (\text{S9})$$

and

$$\mathfrak{S}(q) = \frac{1}{L} \sum_{k,j} e^{-iq(j-k)} \langle \mathbf{S}_k \cdot \mathbf{S}_j \rangle, \quad (\text{S10})$$

respectively. If in Eq. (S9) the generic charge operator is  $\mathcal{N}_i = n_i$ , then the structure factor  $N(q)$  is obtained. If instead the

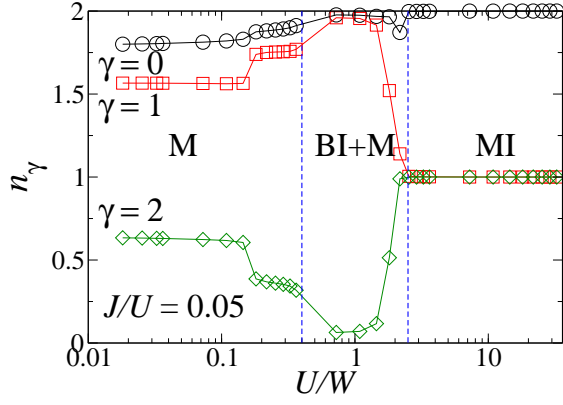


FIG. S4. Mean value of the occupancy corresponding to orbital  $\gamma$ ,  $n_\gamma$ , as a function of the local repulsion  $U$  in units of the bandwidth  $W$ , at a fixed  $J/U = 0.05$ . The phase BI+M is present in the range  $0.4 < U/W < 2$ . The model used is Model 1

definition  $\mathcal{N}_i = n_i^c$  is used, then  $N_c(q)$  is obtained. If in Eq. (S10), the total spin operator  $\mathcal{S}_i = \mathbf{S}_i$  and the “localized” spin operator  $\mathcal{S}_i = \mathbf{S}_i^f$  are inserted, then the corresponding Fourier transforms  $S(q)$  and  $S_f(q)$ , respectively, are obtained. For the case of spin operators, the spatial spin correlations shown in the main text are calculated as the average over their respective correlations at a fixed distance  $d$  [7], namely,

$$S(d) = \frac{1}{L-d} \sum_{j=1}^{L-d} \langle \mathbf{S}_j \cdot \mathbf{S}_{j+d} \rangle. \quad (\text{S11})$$

The charge gap is given as the difference of energies as

$$\Delta_C = E_0(N+1) + E_0(N-1) - 2E_0(N), \quad (\text{S12})$$

where  $E_0(N)$  is identified as the ground state energy of the system with  $N$  particles.

#### S4. ADDITIONAL RESULTS FOR MODEL 1

In this section, additional results are presented corresponding to the FM phase of the OSMF regime and also for the BI+M phase observed at lower values of  $J/U$  and in the intermediate range  $U/W \sim 1$ , since both states were not analyzed in detail in the main text. Only additional results for Model 1 are presented in this supplementary material, but similar results were found for Model 2.

Figure S4 shows the particle occupation number at each orbital vs.  $U/W$ , at a fixed (relatively small)  $J/U = 0.05$  and  $L = 24$  sites. At small  $U/W < 0.4$ , a metallic region is expected with each orbital being partially occupied. In the other extreme, i.e. in the strong coupling regime ( $U/W > 4$ ), clear signatures of a full Mott insulating phase are found with all the occupations being integers. In the intermediate regime of couplings, a phase that can be considered as a slightly doped band insulator was observed. This phase was called BI+M since there is a clear dominance of a “correlated” band insulator state (finite  $U/W$ ) together with metallic fluctuations.

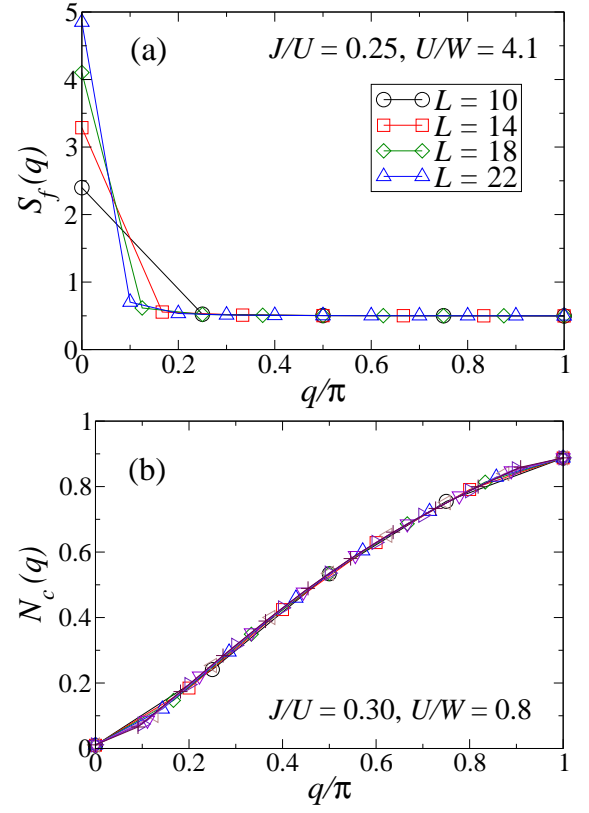


FIG. S5. Localized-band spin and itinerant charge structure factors in the (a) FM and (b) B phases, respectively, for different values of the couplings ( $J/U, U/W$ ) and system sizes. For  $S_f(q)$ , clear signatures of robust FM are found. For  $N_c(q)$ , a broad momentum distribution is observed. The model used is Model 1.

Here, the orbital occupations are not integers but close to integers.

In Fig. S5 (a), the “localized” spin structure factor,  $S_f(q)$ , for the FM phase is shown for different lattice sizes at fixed coupling constants,  $J/U = 1/4$  and  $U/W = 4.1$ . As can be observed from the figure, a robust peak at  $q = 0$  develops indicating the presence of FM order within the OSMF state. Note that the height of this peak increases as  $L$  increases, suggesting a dominant power-law decaying long-range magnetic order in this one dimensional system, as discussed in the main text. The spatial correlation function (not shown) also displays clear FM features, as expected.

In Fig. S5 (b), the “itinerant” charge structure factor,  $N_c(q)$ , is shown for several system lengths, at  $J/U = 0.3$  and  $U/W = 0.8$ . As can be observed in the phase diagram of Model 1, this choice of parameters corresponds to the Block (B) magnetic phase in the OSMF regime. The magnetic structure factor of this phase has already been discussed in the main text. As shown in Fig. S5 (b), the charge in the itinerant bands within the OSMF regime corresponds to that of spinless fermions with a broad momentum distribution, as also discussed in the main text. This behavior is in agreement with previous results reported in numerical studies of the Kondo lattice model [8–10].

Finally, in Fig. S6 the Model 1 orbital occupation is shown



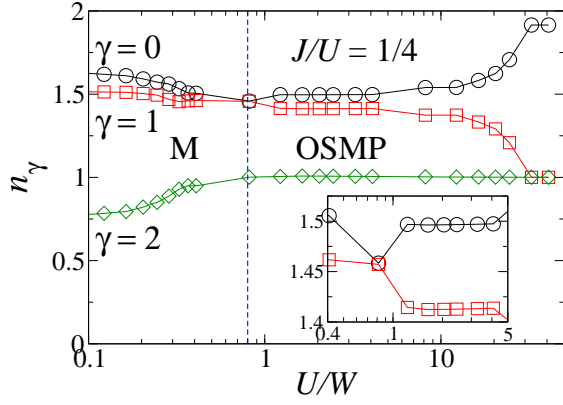


FIG. S6. Results for Model 1: Mean value of the electronic occupancy,  $n_\gamma$ , corresponding to orbital  $\gamma$  vs. the local repulsion  $U/W$  in bandwidth  $W$  units at  $J/U = 1/4$ . The total electronic density corresponds to 2 holes added to the system, as compared with the results shown in Fig.3 (a) for the undoped  $n = 4/3$  case. Inset: detail of  $n_\gamma$  vs.  $U/W$  in the OSMP regime.

for a case identical to that presented in the main text for  $n = 4/3$ , but with two holes added. The purpose of this study is to confirm that the electronic densities  $n_1 \sim n_2 \sim 1.5$  observed in Fig. 3 (main text) change with doping while  $n_2$  remains equal to 1.0 in the OSMP regime. As shown in Fig. S6, indeed this occurs suggesting that the regime observed in our study is compatible with the properties of the OSMP. Moreover, the inset also shows that the electronic densities  $n_0$  and  $n_1$  while very close in value are not identical. In the OSMP regime that starts at  $U/W \sim 1$ , the effect of the original energy splitting between orbitals 0 and 1 diminishes as  $U/W$  further grows and these orbitals become quasi degenerate in the OSMP.

- 
- [1] S. R. White, Phys. Rev. Lett. **69**, 2863 (1992); *ibid.* **48**, 10345 (1993).
  - [2] U. Schollwöck, Rev. Mod. Phys. **77**, 259 (2005).
  - [3] K. Hallberg, Adv. Phys. **55**, 477 (2006).
  - [4] Similar small size effects were reported before in H. Sakamoto and T. Momoi, and K. Kubo, Phys. Rev. B **65**, 224403 (2002).
  - [5] Clear spin order patterns as observed in Fig. S3(c) have been obtained only for particular values of  $(J/U, U/W)$ , while for other couplings the spin order appears more complicated. This could be due to finite size effects, which sometimes occurs if the characteristic length of the stable pattern is not commensurate with the length of the chain  $L$ . Thus, further refinements of our analysis may lead to Block states with even more complex spin

- order patterns as those shown in this publication. In spite of this caveat, the presence of spin order tendencies in the OSMP regime is clear.
- [6] H. Tsunetsugu, M. Sigrist, and K. Ueda, Rev. Mod. Phys. **69**, 809 (1997).
- [7] J. C. Xavier, G. Alvarez, A. Moreo, and E. Dagotto, Phys. Rev. B **81**, 085106 (2010).
- [8] D. J. García, K. Hallberg, C. D. Batista, M. Avignon, and B. Alascio, Phys. Rev. Lett. **85**, 3720 (2000).
- [9] D. J. Garcia, K. Hallberg, C. D. Batista, S. Capponi, D. Poilblanc, M. Avignon, and B. Alascio, Phys. Rev. B **65**, 134444 (2002).
- [10] D. J. Garcia, K. Hallberg, B. Alascio, and M. Avignon, Phys. Rev. Lett. **93**, 177204 (2004).